

## Probing ultrafast spin dynamics with high-harmonic magnetic circular dichroism spectroscopy

F. Willems,<sup>1,2,\*</sup> C. T. L. Smeenk,<sup>2</sup> N. Zhavoronkov,<sup>2</sup> O. Kornilov,<sup>2</sup> I. Radu,<sup>1</sup> M. Schmidbauer,<sup>3</sup> M. Hanke,<sup>4</sup>  
C. von Korff Schmising,<sup>1,2,\*†</sup> M. J. J. Vrakking,<sup>2</sup> and S. Eisebitt<sup>1,2,\*</sup>

<sup>1</sup>*Technische Universität Berlin, Institut für Optik und Atomare Physik, 10623 Berlin, Germany*

<sup>2</sup>*Max-Born-Institut, Max-Born-Strasse 2A, 12489 Berlin, Germany*

<sup>3</sup>*Leibniz-Institut für Kristallzüchtung, Max-Born-Strasse 2, 12489 Berlin, Germany*

<sup>4</sup>*Paul-Drude-Institut für Festkörperelektronik, Hausvogteiplatz 5-7, 10117 Berlin, Germany*

(Received 16 September 2015; revised manuscript received 9 November 2015; published 7 December 2015)

Magnetic circular dichroism in the extreme ultraviolet (XUV) spectral range is a powerful technique for element-specific probing of magnetization in multicomponent magnetic alloys and multilayers. We combine a high-harmonic generation source with a  $\lambda/4$  phase shifter to obtain circularly polarized XUV femtosecond pulses for ultrafast magnetization studies. We report on simultaneously measured resonant magnetic circular dichroism (MCD) of Co and Ni at their respective  $M_{2,3}$  edges and of Pt at its O edge, originating from interface magnetism. We present a time-resolved MCD absorption measurement of a thin magnetic Pt/Co/Pt film, showing simultaneous demagnetization of Co and Pt on a femtosecond time scale.

DOI: [10.1103/PhysRevB.92.220405](https://doi.org/10.1103/PhysRevB.92.220405)

PACS number(s): 75.78.Jp, 42.65.Ky, 75.25.-j, 78.20.Ls

All-optical control and manipulation of magnetization in thin magnetic films is a promising route for spintronics and next-generation magnetic data storage [1,2]. A recent breakthrough demonstrated all-optical switching of magnetization for a technologically important class of ferromagnetic thin films including Co/Pt multilayers with perpendicular magnetic anisotropy [3]. While the role of the Co/Pt interface is not yet well understood, the enhanced spin-orbit interaction at the interface has been shown to lead to a significant acceleration of the demagnetization rate [4]. Furthermore, in heterogeneous samples, laser-induced superdiffusive spin currents can contribute to the ultrafast magnetization dynamics [5–7] by leading to spin accumulation at paramagnetic/magnetic interfaces [8]. Also, optical control of spin-polarized currents has been demonstrated at Co/Pt heterostructures promising new applications in spintronics in the terahertz regime [9]. However, progress in understanding and, hence, in the successful design of such new multicomponent magnetic systems for ultrafast applications has been challenged by the difficulty to experimentally access the underlying complex microscopic processes. Our novel technique presented here, combines femtosecond time resolution with element-specific probing, which is a prerequisite for extracting information about contributions of the different materials and interacting spin systems.

Time-resolved x-ray magnetic circular dichroism (XMCD) experiments, using soft x-rays, have been pioneered at the synchrotron facility BESSY II, HZB, using the so-called slicing scheme [10]. While significant success has been achieved with this method [11,12], important shortcomings are the low photon flux and limited temporal resolution of  $> 120$  fs. Furthermore, at synchrotron undulator sources the photon energy must be tuned across the resonances of the constituent elements, making it impossible to simultaneously probe spin dynamics of different elements in the sample. On the other

hand, laser-based high-order harmonic generation (HHG) techniques have recently been used to observe magnetization dynamics using the transverse magneto-optic Kerr effect in a reflection geometry [7,13–15]. While this technique offers excellent time resolution, its very broad spectral response makes element-specific studies challenging. In addition, it has triggered a controversy about the extent that ultrafast changes of the index of refraction may complicate the relationship between the asymmetry of the reflected intensity and the actual magnetization [16–18]. Finally, progress has been made by generating circularly polarized extreme ultraviolet (XUV) radiation with two-color counter-rotating circularly polarized [19,20] or two-color oppositely linearly polarized laser pulses [21]. In the latter study, circular polarization was experimentally demonstrated via *static* Ni  $M$ -edge magnetic circular dichroism (MCD) measurements.

Here we demonstrate time-resolved, multielement MCD absorption spectroscopy of several distinct elements in a single measurement with high-order harmonic radiation covering the  $M_{2,3}$  edges of  $3d$  transition-metal atoms (40–72 eV). We employ a reflection-based polarizer to efficiently produce circularly polarized femtosecond XUV pulses and present both static MCD measurement of a thin Co/Ni/Pt and Pt/Co/Pt films as well as a time-resolved MCD measurement of the magnetization dynamics in the latter sample. We observe the decay of the interface magnetization in Pt simultaneously with the demagnetization of Co after optical excitation. Our results demonstrate element-specific sensitivity of broadband MCD absorption spectroscopy in studies of ultrafast demagnetization. Our work represents a significant advancement towards the development of tabletop systems for element-specific spectroscopy and imaging of chiral-sensitive light-matter interaction with nanometer spatial and femtosecond temporal resolution.

The experimental setup is shown schematically in Fig. 1. 35 fs pulses from a Ti:sapphire laser system operating at 1 kHz repetition rate and a central wavelength of 795 nm are split into pump and probe beams by a thin beam splitter. The 2 mJ pulse in the probe arm is focused at  $f/115$  into a 5-mm-long gas cell containing neon. The strongly nonlinear

\*Present address: Max-Born-Institut, Max-Born-Strasse 2A, 12489 Berlin, Germany.

†Korff@mbi-berlin.de

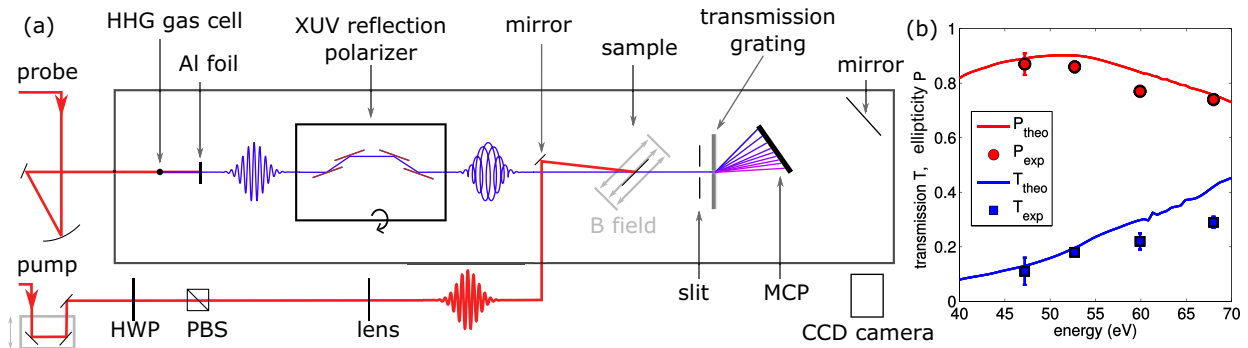


FIG. 1. (Color online) (a) Schematic of the experimental setup. The IR pulse enters the vacuum chamber (black box) and drives HHG in the gas cell. The driving IR pulse is removed by a 300 nm Al foil. Transmitted XUV pulses (blue line) are converted to circular polarization by the reflection XUV polarizer. The sample holder has a built-in electromagnet used to change the direction of the external magnetic field applied to the sample. The high-harmonic spectrum transmitted through the sample is recorded by an XUV spectrometer [22]. The pump-probe delay is controlled using a delay stage. (b) Measured and calculated ellipticity (red, circles) and transmission (blue, squares) of the reflection XUV polarizer over the spectral range covering the  $M$  edges of 3d transition metals.

light-matter interaction in the cell leads to generation of XUV pulses via high-harmonic generation [23,24]. The polarization of the emitted XUV pulses is initially linear and parallel to the polarization of the infrared driving pulse. The driving IR light is blocked by a 300-nm-thick Al foil, which transmits  $\sim 50\%$  of the XUV light up to the Al  $L_3$  edge at 72.5 eV.

Following the filter, the linearly polarized XUV pulses enter the reflection XUV polarizer [25–28]. Two parameters control the polarization and transmission of the XUV pulse: (i) the angle of incidence and (ii) the rotation angle of the four-mirror assembly around the beam axis, controlling the ratio of the  $s$  and  $p$  components incident on the mirrors. The optimal performance over a wide range of photon energies is achieved with a Mo(20 nm)/ $B_4C$ (2 nm) mirror coating and a fixed angle of incidence of  $78^\circ$ . While a higher degree of ellipticity of  $P \sim 1$  can be easily realized by using larger incident angles, the transmission in this case is significantly reduced. The performance of the polarizer was characterized at a synchrotron facility (HZB, BESSY II, UE112). As shown in Fig. 1(b), the device nearly reaches the theoretically predicted degrees of polarization and transmission. The ellipticity is  $>0.75$  and the transmission is around 20% over the energy range of interest of 40–70 eV, which spans the  $M$  edges of the 3d ferromagnetic transition metals (Fe, Co, and Ni).

The elliptically polarized XUV pulses impinge upon an in-plane magnetized ferromagnetic sample mounted on a manipulator with a built-in electromagnet. For a nonzero projection of the magnetization on the incoming wave vector  $\vec{k}$  of the XUV probe pulses, the samples are mounted under  $45^\circ$  incident angle. A magnetic field of  $B_\pm = \pm 30$  mT is sufficient to fully saturate the magnetization of the samples used in the experiment. At the sample, the probe is recombined with the linearly polarized pump pulse in a noncollinear geometry. The angle between the pump and probe beams is  $6^\circ$ . The photon flux of the pump pulse is controlled using a half-waveplate (HWP) and a polarizing beam splitter (PBS). The pump beam is focused at  $f/150$  just slightly beyond the sample using a lens outside the vacuum chamber to ensure that the area probed by the XUV pulse is uniformly illuminated by the pump pulse. The time resolution of the experiment is

determined by an all-optical cross-correlation in a nonlinear crystal giving an upper limit of  $\tau_G = (59 \pm 5)$  fs. The XUV light transmitted through the sample is recorded by an XUV spectrometer. The spectrometer contains a  $50 \mu\text{m}$  slit followed by a transmission nanograting [22], resulting in a spectral resolution of approximately 0.75 eV at 60 eV. The slit selects a small portion ( $30 \mu\text{rad}$  angular width) of the divergent XUV radiation produced in the HHG cell. The spectrally dispersed XUV light is detected by a microchannel plate/phosphor screen assembly and is imaged using a CCD camera.

Two thin-film samples are studied in the present experiment. They are grown by dc magnetron sputtering on 20-nm-thin XUV-transparent  $\text{Si}_3\text{N}_4$  membranes with dimensions of  $0.25 \times 1 \text{ mm}^2$  on silicon supporting frames. The first sample consists of  $\text{Si}_3\text{N}_4/\text{Pt}(6 \text{ nm})/\text{Co}(15 \text{ nm})/\text{Pt}(2 \text{ nm})$  layers, and the second magnetic bilayer sample is  $\text{Si}_3\text{N}_4/\text{Co}(15 \text{ nm})/\text{Ni}(15 \text{ nm})/\text{Pt}(2 \text{ nm})$ . The samples are carefully characterized by magneto-optical Kerr measurements, spatially resolved x-ray reflectivity measurements before and after laser excitation, energy-dispersive x-ray analysis, static x-ray absorption (XAS), and static MCD measurements (see below).

Transmitted XUV spectra for two opposite directions of the external magnetic field applied to both samples,  $B_\pm$ , are shown in Figs. 2(a) and 2(b). These spectra are averaged over 170 s for each magnetic field direction. The relative root-mean-square intensity fluctuations within one harmonic and an integration time of 10 s are typically on the order of 2%. For the Pt/Co/Pt sample, harmonic 39 (60.8 eV) shows the largest dichroism corresponding to the  $M_{2,3}$  edge of Co [Fig. 2(a)]; in the Co/Ni/Pt bilayer sample, an additional dichroic effect at harmonic 43 (=67.1 eV) is visible corresponding to the  $M_{2,3}$  edge of Ni, demonstrating simultaneous measurement of the magnetization of two elements present in the sample. In addition, the spectrum in Fig. 2(a) shows a weaker dichroic signal at 54.6 eV (harmonic 35), which will be discussed below. The insets of Figs. 2(a) and 2(b) show XAS and MCD signals recorded at the synchrotron facility (HZB, BESSY II, PM3) for the two samples. For the Co/Ni/Pt sample the pronounced absorption peaks and MCD signals [red and black

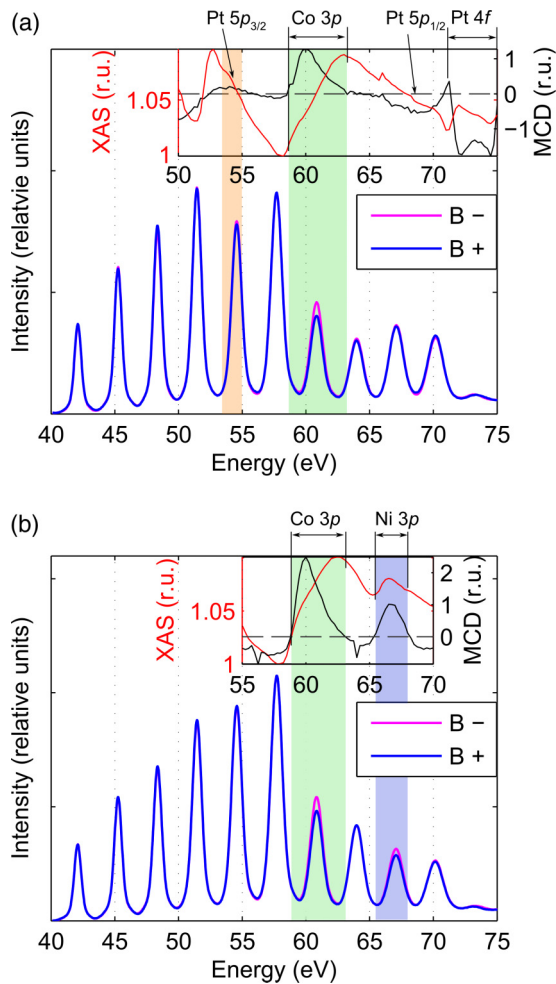


FIG. 2. (Color online) Static high-order harmonic spectrum for two opposite magnetization directions ( $B_+$ ,  $B_-$ ) of sample (a) Pt/Co/Pt and (b) Co/Ni/Pt. Pronounced dichroic absorption is observed at the  $M_{2,3}$  edges of Co (60.8 eV) and Ni (67.1 eV). The inset shows XAS (red line) and MCD (black line) spectra measured with circularly polarized synchrotron radiation. In these measurements, we can clearly identify the absorption peaks and the magnetic asymmetry at the  $M_{2,3}$  edge. Additionally, for the Pt/Co/Pt sample, the absorption and MCD signal of the  $5p$  (O) and  $4f$  (N) transitions of Pt are identified.

lines in Fig. 2(b)] at the Co and Ni  $M_{2,3}$  edge are at 60.0 and 66.5 eV, respectively [29,30], and in very good agreement with our HHG measurements. The Pt/Co/Pt sample shows a more complicated spectrum. In addition to the XAS and MCD signal at the Co  $M_{2,3}$  edge ( $3p \rightarrow 3d$ ), we observe absorption peaks in the XAS spectrum and corresponding contributions in the MCD spectrum stemming from Pt  $N_{6,7}$  ( $4f_{5/2,7/2} \rightarrow 5d$ ) as well as from the Pt  $O_{2,3}$  edge ( $5p_{1/2,3/2} \rightarrow 5d$ ) [see inset of Fig. 2(a)]. This finding is in good qualitative agreement with an experimental work by Shishidou *et al.* [31], that measured XAS and MCD spectra of a CoPt<sub>3</sub> alloy in the same energy range. The MCD signals of paramagnetic Pt are caused by hybridization of Co  $3d$  and Pt  $5d$  orbitals, leading to a considerable magnetic polarization of Pt, highly localized within a few monolayers at the Co/Pt interfaces [32,33]. The MCD signal detected in the HHG transmission

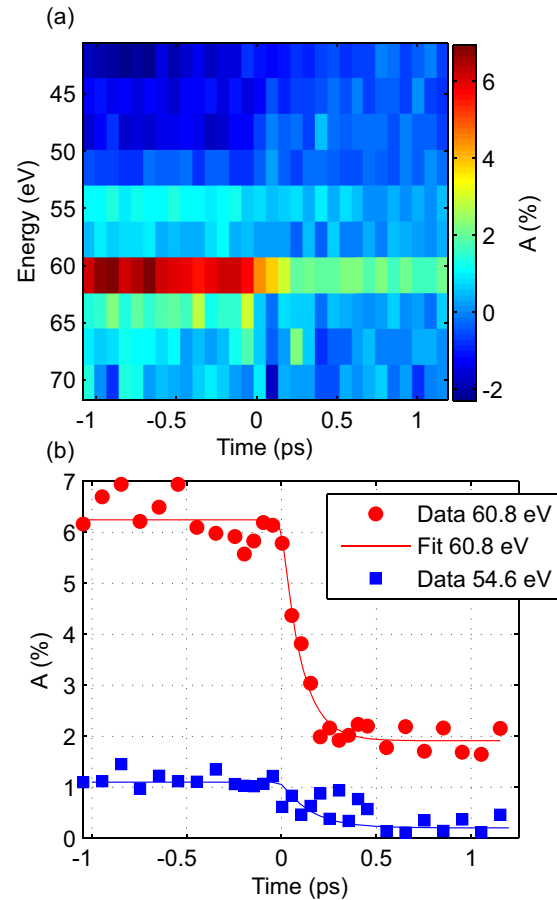


FIG. 3. (Color online) (a) Time-resolved magnetic asymmetry,  $A$ , as a function of probing energy and delay time of the Pt/Co/Pt layer. (b) Time-resolved MCD dynamics around the  $M_{2,3}$  edge of Co (60.8 eV) with nonlinear least-square fit using Eq. (1) (solid, red line), and Pt  $O_3$  edge (54.6 eV) with the solid, blue line to guide the eye.

spectrum at 54.6 eV [also compare Fig. 3(a)] can hence be clearly associated with the strong absorption at the Pt  $O_3$  edge. The pronounced dichroic signal of the  $4f$  electrons of Pt is cut in the HHG spectrum by the aluminum filter ( $L_3$  at 72.5 eV). To exclude interdiffusion of the Co and Pt layers induced by the IR laser excitation we performed spatially resolved x-ray reflectivity measurements with a micrometer-sized x-ray beam ( $10 \times 200 \mu\text{m}^2$ ) at a synchrotron facility [HZB, BESSY II, U125/2-KMC,  $E = 9.985$  keV, Si(111) monochromator with  $\Delta E/E = 10^{-4}$ ]. Careful comparison of measurements between the laser excited region on the  $\text{Si}_3\text{N}_4$  membrane and on the silicon wafer show no significant difference; strongly modulated Kiessig fringes demonstrate an unchanged density contrast and an intact layered structure of the Pt/Co/Pt sample.

In time-resolved experiments we observe ultrafast demagnetization of the Pt/Co/Pt after excitation with an IR pump pulse of  $\approx 6$  mJ/cm<sup>2</sup>. The magnetic asymmetry,  $A = (I_{B_+} - I_{B_-}) / (I_{B_+} + I_{B_-})$ , is calculated from the HHG spectra by integrating the signal intensity  $I_{B_{\pm}}$  over each harmonic peak to improve the signal-to-noise ratio at the expense of spectral resolution. Pronounced ultrafast changes in the

magnetic asymmetry are observed as a function of pump-probe delay, as shown in Fig. 3(a) for the energy range of 40–70 eV. We observe a constant magnetic asymmetry for negative time delays of approximately  $A \approx 6\%$  at the Co edge at 60.8 eV. Immediately after the optical pump pulse arrives, the magnetic asymmetry decreases to approximately 2%, tracking the loss of magnetization in the Co film. The signal of the adjacent harmonic at 64 eV displays similar dynamics and is a consequence of the Co resonance extending into this energy range, as can be seen in the inset of Fig. 2(a). The magnetic asymmetry in the harmonic peak centered at 54.6 eV, attributed to the Pt O<sub>3</sub> edge, also shows a dependence on the pump-probe delay. In Fig. 3(b) we show the time-resolved traces for two selected energies probing the Co and Pt response. The trace at 60.8 eV depicts the ultrafast magnetization dynamics of Co, well described by a monoexponential decay function with a time constant of  $\tau_{\text{Co}} = (92 \pm 22)$  fs, convoluted with a Gaussian,  $\Gamma(t, \tau_G)$ , to reflect the finite temporal resolution with a full width at half maximum of  $\tau_G = 59$  fs.  $\Theta(t)$  is the step function at  $\Delta t = 0$ , and  $\Delta A$  is the maximal change in the magnetic asymmetry.

$$A(t) = [A(t < 0) + (\Delta A)(e^{-t/\tau_{\text{Co}}} - 1)\Theta(t)] \otimes \Gamma(t, \tau_G). \quad (1)$$

The observed demagnetization time constant,  $\tau_{\text{Co}}$ , is shorter in comparison with recent optical Kerr measurements of pure Co films with comparable demagnetization amplitudes [4,34]. On the other hand, magnetization studies in the XUV energy range in magnetic heterogeneous samples revealed comparable time constants of 100 fs [35,36]. It remains an open and challenging question, in how far these significantly deviating demagnetization times reported in literature are related to differences in the probing mechanism [37,38] or may be caused by differences in the geometry of the sample layout, e.g., effects due to spin transport [5] or enhanced spin-orbit coupling at interfaces [4].

The MCD feature at 54.6 eV shows, within the statistical noise, a comparable ultrafast temporal behavior suggesting that the magnetic polarization in Pt is quenched simultaneously with the loss of magnetization in the Co layer. Also, Co and Pt show a similar relative demagnetization amplitude. In light of recently discussed ultrafast magnetization effects at ferromagnetic/paramagnetic interfaces [4,8,9], this represents an interesting experimental scenario, which deserves further discussion. Laser excited, nonequilibrium electrons in ferromagnetic materials have spin-dependent lifetimes and velocities, leading to a redistribution of magnetization in thin multilayered magnetic systems [6,7]. Additionally, at interfaces between two different materials the electron transport

properties abruptly change and can lead to spin accumulation [5]: majority spin states in Co are *sp*-like with high band velocities, while electrons in Pt will fill more localized *d* states, with much slower propagation and an increased scattering. This has been shown in a recent experimental and theoretical work where a considerable amount of magnetization was transferred from a thin ferromagnetic film to the interface region of an adjacent paramagnetic layer [8]. On the other hand, experimental results are in agreement with the hypothesis that an enhanced spin-orbit coupling at Co/Pt interfaces leads to increased Elliott-Yafet spin-flip scattering and therefore to a faster and more efficient demagnetization process [4]. Hence, such possibly competing microscopic processes at interfaces may result in both distinct magnetization dynamics and distinct transient magnetization amplitudes. While for the experimental parameters described here our results suggest that these processes do not contribute dominantly, we envision that time-resolved, broadband MCD measurements will be the ideal tool for further detailed studies of optically induced dynamics of interface magnetism.

In conclusion, we have implemented the first laboratory-based, femtosecond time-resolved, broadband MCD setup, which allows the simultaneous observation of ultrafast demagnetization dynamics with element specificity in multicomponent magnetic samples. The performance of the setup in static configuration is demonstrated by measuring MCD effects in Pt/Co/Pt and Co/Ni/Pt samples. We observe asymmetry signals due to magnetization of the Co and Ni layers as well as due to induced interfacial magnetization of Pt. We present a time-resolved MCD study of a Pt/Co/Pt sample pumped by a femtosecond IR pulse showing femtosecond demagnetization of the Co layer on a time scale of  $(92 \pm 22)$  fs. Similar demagnetization dynamics are observed at the Pt O<sub>3</sub> edge suggesting that the Co/Pt interface directly follows the magnetization of the Co layer.

Finally, we envision that the availability of circularly polarized XUV radiation demonstrated here will allow coherent imaging and holographic techniques of magnetic nanostructures [35,39,40] with a laboratory-based tabletop system with femtosecond temporal and nanometer spatial resolution.

We gratefully acknowledge Paul Frömmel and Martin Eckstein for their decisive contributions in the construction of the HHG setup used in the present experiments. S.E. and F.W. thank the Helmholtz Virtual Institute VH-VI-419 “Dynamic Pathways in Multidimensional Landscapes” for support. We thank Helmholtz-Zentrum Berlin (HZB) for the allocation of synchrotron radiation beamtime.

- 
- [1] A. Kirilyuk, A. V. Kimel, and T. Rasing, *Rep. Prog. Phys.* **76**, 026501 (2013).
- [2] S. Mangin, M. Gottwald, C.-h. Lambert, D. Steil, V. Uhlíř, L. Pang, M. Hehn, S. Alebrand, M. Cinchetti, G. Malinowski, Y. Fainman, M. Aeschlimann, and E. E. Fullerton, *Nat. Mater.* **13**, 286 (2014).
- [3] C.-H. Lambert, S. Mangin, B. S. D. C. S. Varaprasad, Y. K. Takahashi, M. Hehn, M. Cinchetti, G. Malinowski, K. Hono, Y. Fainman, M. Aeschlimann, and E. E. Fullerton, *Science* **345**, 1337 (2014).
- [4] K. C. Kuiper, T. Roth, A. J. Schellekens, O. Schmitt, B. Koopmans, M. Cinchetti, and M. Aeschlimann, *Appl. Phys. Lett.* **105**, 202402 (2014).
- [5] M. Battiato, K. Carva, and P. M. Oppeneer, *Phys. Rev. Lett.* **105**, 027203 (2010).
- [6] D. Rudolf, C. La-O-Vorakiat, M. Battiato, R. Adam, J. M. Shaw, E. Turgut, P. Maldonado, S. Mathias, P. Grychtol, H. T. Nembach, T. J. Silva, M. Aeschlimann, H. C. Kapteyn, M. M. Murnane, C. M. Schneider, and P. M. Oppeneer, *Nat. Commun.* **3**, 1037 (2012).

- [7] E. Turgut, C. La-o-vorakiat, J. M. Shaw, P. Grychtol, H. T. Nembach, D. Rudolf, R. Adam, M. Aeschlimann, C. M. Schneider, T. J. Silva, M. M. Murnane, H. C. Kapteyn, and S. Mathias, *Phys. Rev. Lett.* **110**, 197201 (2013).
- [8] T. Kampfprath, M. Battiato, P. Maldonado, G. Eilers, J. Nötzold, S. Mährlein, V. Zbarsky, F. Freimuth, Y. Mokrousov, S. Blügel, M. Wolf, I. Radu, P. M. Oppeneer, and M. Münzenberg, *Nat. Nanotechnol.* **8**, 256 (2013).
- [9] T. J. Huisman, R. V. Mikhaylovskiy, J. D. Costa, F. Freimuth, E. Paz, J. Ventura, P. P. Freitas, S. Blügel, Y. Mokrousov, Th. Rasing, and A. V. Kimel, [arXiv:1505.02970v1](https://arxiv.org/abs/1505.02970v1).
- [10] K. Holldack, J. Bahrtdt, A. Balzer, U. Bovensiepen, M. Brzhezinskaya, A. Erko, A. Eschenlohr, R. Follath, A. Firsov, W. Frentrop, L. Le Guyader, T. Kachel, P. Kuske, R. Mitzner, R. Müller, N. Pontius, T. Quast, I. Radu, J.-S. Schmidt, C. Schüßler Langeheine *et al.*, *J. Synchrotron Radiat.* **21**, 1090 (2014).
- [11] C. Stamm, T. Kachel, N. Pontius, R. Mitzner, T. Quast, K. Holldack, S. Khan, C. Lupulescu, E. F. Aziz, M. Wietstruk, H. A. Dürr, and W. Eberhardt, *Nat. Mater.* **6**, 740 (2007).
- [12] I. Radu, K. Vahaplar, C. Stamm, T. Kachel, N. Pontius, H. A. Dürr, T. A. Ostler, J. Barker, R. F. L. Evans, R. W. Chantrell, A. Tsukamoto, A. Itoh, A. Kirilyuk, Th. Rasing, and A. V. Kimel, *Nature (London)* **472**, 205 (2011).
- [13] C. La-O-Vorakiat, M. Siemens, M. M. Murnane, H. C. Kapteyn, S. Mathias, M. Aeschlimann, P. Grychtol, R. Adam, C. M. Schneider, J. M. Shaw, H. Nembach, and T. J. Silva, *Phys. Rev. Lett.* **103**, 257402 (2009).
- [14] C. La-O-Vorakiat, E. Turgut, C. A. Teale, H. C. Kapteyn, M. M. Murnane, S. Mathias, M. Aeschlimann, C. M. Schneider, J. M. Shaw, H. T. Nembach, and T. J. Silva, *Phys. Rev. X* **2**, 011005 (2012).
- [15] S. Mathias, C. La-O-Vorakiat, P. Grychtol, P. Granitzka, E. Turgut, J. M. Shaw, R. Adam, H. T. Nembach, M. E. Siemens, S. Eich, C. M. Schneider, T. J. Silva, M. Aeschlimann, M. M. Murnane, and H. C. Kapteyn, *Proc. Natl. Acad. Sci. USA* **109**, 4792 (2012).
- [16] B. Vodungbo, J. Gautier, G. Lambert, P. Zeitoun, and J. Lüning, *Phys. Rev. X* **3**, 038001 (2013).
- [17] I. Radu, C. Stamm, A. F. Radu, R. Abrudan, K. Vahaplar, T. Kachel, N. Pontius, R. Mitzner, K. Holldack, A. Föhlisch, T. A. Ostler, J. H. Mentink, R. F. L. Evans, R. W. Chantrell, A. Tsukamoto, A. Itoh, A. Kirilyuk, A. V. Kimel, and Th. Rasing, *Spin* **5**, 1550004 (2015).
- [18] D. Hinzke, U. Atxitia, K. Carva, P. Nieves, O. Chubykalo-Fesenko, P. M. Oppeneer, and U. Nowak, *Phys. Rev. B* **92**, 054412 (2015).
- [19] O. Kfir, P. Grychtol, E. Turgut, R. Knut, D. Zusin, D. Popmintchev, T. Popmintchev, H. Nembach, J. M. Shaw, A. Fleischer, H. Kapteyn, M. Murnane, and O. Cohen, *Nat. Photonics* **9**, 99 (2014).
- [20] A. Fleischer, O. Kfir, T. Diskin, P. Sidorenko, and O. Cohen, *Nat. Photonics* **8**, 543 (2014).
- [21] G. Lambert, B. Vodungbo, J. Gautier, B. Mahieu, V. Malka, S. Sebban, P. Zeitoun, J. Lüning, J. Perron, A. Andreev, S. Stremoukhov, F. Ardana-Lamas, A. Dax, C. P. Hauri, A. Sardinha, and M. Fajardo, *Nat. Commun.* **6**, 6167 (2015).
- [22] O. Kornilov, R. Wilcox, and O. Gessner, *Rev. Sci. Instrum.* **81**, 063109 (2010).
- [23] A. L'Huillier, K. J. Schafer, and K. C. Kulander, *J. Phys. B: At., Mol. Opt. Phys.* **24**, 3315 (1991).
- [24] P. B. Corkum, *Phys. Rev. Lett.* **71**, 1994 (1993).
- [25] D. Wilson, D. Rudolf, C. Weier, R. Adam, G. Winkler, R. Frömter, S. Danylyuk, K. Bergmann, D. Grützmacher, C. M. Schneider, and L. Juschkin, *Rev. Sci. Instrum.* **85**, 103110 (2014).
- [26] B. Vodungbo, A. Barszczak Sardinha, J. Gautier, G. Lambert, C. Valentin, M. Lozano, G. Iaquaniello, F. Delmotte, S. Sebban, J. Lüning, and P. Zeitoun, *Opt. Express* **19**, 4346 (2011).
- [27] H. Höchst and F. Middleton, *Nuclear Instrum. Methods Phys. Rese.* **347**, 107 (1994).
- [28] H. Höchst, D. Zhao, and D. L. Huber, *Surf. Sci.* **352-354**, 998 (1996).
- [29] J. C. Fuggle and N. Mårtensson, *J. Electron Spectrosc. Relat. Phenom.* **21**, 275 (1980).
- [30] S. Valencia, A. Gaupp, W. Gudat, H. C. Mertins, P. M. Oppeneer, D. Abramsohn, and C. M. Schneider, *New J. Phys.* **8**, 254 (2006).
- [31] T. Shishidou, S. Imada, T. Muro, F. Oda, A. Kimura, S. Suga, T. Miyahara, T. Kanomata, and T. Kaneko, *Phys. Rev. B* **55**, 3749 (1997).
- [32] F. Wilhelm, P. Pouloupoulos, A. Scherz, H. Wende, K. Baberschke, M. Angelakeris, N. K. Flevaris, J. Goulon, and A. Rogalev, *Phys. Status Solidi A* **196**, 33 (2003).
- [33] N. Nakajima, T. Koide, T. Shidara, H. Miyauchi, H. Fukutani, A. Fujimori, K. Iio, T. Katayama, M. Nývlt, and Y. Suzuki, *Phys. Rev. Lett.* **81**, 5229 (1998).
- [34] B. Koopmans, G. Malinowski, F. Dalla Longa, D. Steiauf, M. Fähnle, T. Roth, M. Cinchetti, and M. Aeschlimann, *Nature Materials* **9**, 259 (2010).
- [35] C. von Korff Schmising, B. Pfau, M. Schneider, C. M. Günther, M. Giovannella, J. Perron, B. Vodungbo, L. Müller, F. Capotondi, E. Pedersoli, N. Mahne, J. Lüning, and S. Eisebitt, *Phys. Rev. Lett.* **112**, 217203 (2014).
- [36] B. Vodungbo, J. Gautier, G. Lambert, A. B. Sardinha, M. Lozano, S. Sebban, M. Ducouso, W. Boutu, K. Li, B. Tudu, M. Tortarolo, R. Hawaldar, R. Delaunay, V. López-Flores, J. Arabski, C. Boeglin, H. Merdji, P. Zeitoun, and J. Lüning, *Nat. Commun.* **3**, 999 (2012).
- [37] K. Carva, M. Battiato, and P. M. Oppeneer, *Nat. Phys.* **7**, 665 (2011).
- [38] A. Weber, F. Pressacco, S. Günther, E. Mancini, P. M. Oppeneer, and C. H. Back, *Phys. Rev. B* **84**, 132412 (2011).
- [39] S. Eisebitt, J. Lüning, W. F. Schlotter, M. Lörger, O. Hellwig, W. Eberhardt and J. Stöhr, *Nature (London)* **432**, 885 (2004).
- [40] S. Schaffert, B. Pfau, J. Geilhufe, C. M. Günther, M. Schneider, C. v. Korff Schmising, and S. Eisebitt, *New J. Phys.* **15**, 093042 (2013).